Surface-Coverage Dependence of Surface-Enhanced Raman Scattering from Gold Nanocubes on Self-Assembled Monolayers of Analyte†

Patrick N. Sisco and Catherine J. Murphy*

Department of Chemistry and Biochemistry, University of South Carolina, Columbia, South Carolina 29208

Received: November 24, 2008; Revised Manuscript Received: February 12, 2009

Surface enhanced Raman scattering (SERS) spectra of 4-mercaptobenzoic acid (4-MBA) self-assembled monolayers (SAMs) on gold substrates are presented for SAMs onto which gold nanocubes have been electrostaticaly immobilized. In the absence of nanocubes, no SERS signals from 4-MBA SAMs are observed. Upon addition of the gold nanocubes to the SAM, a sandwich architecture is formed, allowing for coupling between the localized surface plasmon of the nanocubes and the surface plasmon of the gold substrate. This creates a large electromagnetic field in the area where the 4-MBA molecules reside, causing the characteristic vibrational modes of 4-MBA to appear. SERS intensities increase linearly with increasing nanocube coverage up to a factor of 7 in the best case studied here, with enhancement factors of up to 10^{13}.

Introduction

Surface enhanced Raman scattering (SERS) spectroscopy is a powerful technique to obtain vibrational information about molecules on or near a nanoscale metallic surface.[1] Since the introduction of SERS on roughened silver electrodes in 1977,[2,3] there has been a great deal of research to maximize the Raman signals from adsorbates on gold and silver substrates. Recent developments in the controlled synthesis of gold and silver nanomaterials of different shapes have led to a renewed interest in SERS.[4−18] For gold and silver, decreasing particle size below the electron mean free path (∼10−100 nm) leads to an intense absorption in the visible−near-infrared region of the electromagnetic spectrum, known as a plasmon resonance.[12] This plasmon resonance produces a large electromagnetic field that extends outward from the nanoparticle surface up to 10 nm, or farther, depending on particle size. The plasmon frequency can be tuned by changing the size, shape, and aggregation state of the nanoparticles.[12,13] Because Raman scattering intensity is proportional to the fourth power of the local electric field, molecules within ∼10 nm of a nanoscale metal surface can have their Raman-active band intensities increase by 6−10 orders of magnitude.[1,14,15] Molecules caught in the junctions between nanoparticles have even larger SERS signal enhancements, because the spatially coincident local electric fields provide "hot spots" for SERS.[16]

Nanoparticles with corners and sharp tips are of significant interest as SERS substrates.[17−19] Local electric field enhancements are seen for all types of noble metal nanoparticles, but even greater local field enhancements are observed at sharp surface features, such as the corners of gold nanocubes, where the curvature radius is much smaller than the size of the nanoparticle.[20] This phenomenon is known as the "lightning rod" effect on surface enhancement.[20,21] This effect has led many researchers to use gold and silver nanomaterials of different morphologies as SERS substrates. The Moskovits laboratory has studied SERS on both aligned silver nanowire rafts[22] and metal−silica hybrid nanostructures.[23] The El-Sayed group has investigated the use of both unaggregated[24] and aggregated[25] gold nanorods as SERS substrates. More recently, the El-Sayed group has shown that human oral cancer cells can align antibody-derivatized gold nanorods on the cell surface, and this nanorod alignment on the cell surface leads to a SERS fingerprint unique to the cancer cells.[26] The Halas group has shown that large enhancement factors of 10^9-10^{10}, compared to normal Raman spectra, can be observed for 4-mercaptoaniline using gold nanoshells.[27] Many complex SERS substrates have also been prepared by the van Duyne group using nanosphere lithography for the quantitative detection of analytes such as glucose and biowarfare agents.[1]

One of the biggest challenges facing SERS on colloidal nanoparticle substrates is reproducibility. It is essential to know both the number of nanoparticles in solution and the number of molecules sampled during the experiment for analyte quantitation and calculation of SERS enhancement factors. This can be difficult for colloidal nanoparticles because the number of molecules in nanoparticle junctions, which could contribute the majority of the signal, is typically unknown. SERS measurements on self-assembled monolayers (SAMs) of the target analyte on planar gold substrates allow for the SAMs to be deposited on a smooth gold surface and allow for the number of molecules sampled to be well-known, but the SERS signals obtained from planar substrates are weak.[17]

Previous reports from this laboratory have demonstrated a colloidal chemistry approach to improve SERS for analytes adsorbed to smooth gold substrates.[17,28] This was based on a nanoparticle−planar substrate sandwich structure in which gold nanoparticles of various shapes and sizes were immobilized on SAMs of 4-mercaptobenzoic acid (4-MBA) on sputtered gold slides. The SERS enhancements seen with this sandwich geometry originate from the plasmon coupling between the localized surface plasmon of the nanoparticles and the surface plasmon of the gold substrate, creating a large local electromagnetic field for the molecules between the planar substrate and the nanoparticles.[17] We found the largest Raman signal enhancements were for gold nanocubes (10^9-fold increase in signal compared to normal Raman of a solution of 4-MBA), as compared to spheres, rods, and other shapes, for which 10^7-10^8 signal enhancements were observed.[17] In our earlier report, the

† Part of the "George C. Schatz Festschrift".

* To whom correspondence should be addressed. E-mail: Murphy@mail.chem.sc.edu.

10.1021/jp810329j CCC: $40.75
Published on Web 03/09/2009

focus was on the effect of the particle shape on the SERS signals, in the condition of "no" junctions between the nanoparticles on the SAM.[17] In this report, we investigate the effects of both an increase in surface coverage and an increase in aggregation of gold nanocubes on the enhancement of the Raman signal for 4-MBA in this sandwich architecture. Our hypothesis was that as aggregation of nanocubes increased, SERS signal intensities from the underlying SAM would increase more than simple surface coverages would predict.

Experimental Section

Materials. Chloroauric acid ($HAuCl_4 \cdot 3H_2O$), sodium borohydride ($NaBH_4$), ascorbic acid, and 4-mercaptobenzoic acid (4-MBA) were obtained from Aldrich. Hexadecyltrimethylammonium bromide (cetyltrimethylammonium bromide, CTAB) was obtained from Sigma as a SigmaUltra pure reagent. All reagents were used as received. Deionized ultrafiltered (DIUF) water was obtained from Fisher and used for all procedures. All glassware was cleaned with aqua regia, rinsed thoroughly with DIUF water, and dried prior to use.

Instrumentation. Surface-enhanced Raman spectra were collected using two different Jobin Yvon Horiba confocal Raman spectrometers. The first is equipped with a p-polarized 632.8 nm HeNe laser with a 2 μm spot size using an 80× objective and 5 mW power at the sample. The second system is equipped with a p-polarized 785 nm laser with a 1 μm spot size using a 100× objective and 7 mW power at the sample. Samples were excited normal to the surface. Absorption spectra of nanoparticles in aqueous solution were acquired using a Cary 500 Scan UV−vis−NIR spectrometer. Zeta potential measurements were performed on a Brookhaven Zeta PALS instrument. Scanning electron micrographs were acquired using an FEI Quanta 200 environmental scanning electron microscope. It is important to note that the Raman spectra and SEM images were acquired on the same sample in approximately the same region to minimize possible effects from sample heterogeneity. Transmission electron microscopy was performed on a Hitachi H-8000 microscope, and electron diffraction data were obtained using a JEOL 2100F HRTEM.

Nanocube Synthesis. Gold nanocubes of edge length 47 ± 3 nm were prepared according to a modified surfactant-directed seed-mediated approach.[29] The seed particles were prepared using a 7.75 mL growth solution containing 0.1 M CTAB and 3.23×10^{-4} M $HAuCl_4$. To this growth solution, 600 μL of an ice cold 0.01 M $NaBH_4$ solution was added. The resulting solution was stirred for 2 min and allowed to sit for one hour before use. The seed solution was diluted by a factor of 10 using DIUF water. For cube synthesis, growth solutions were prepared that contained 4 mL of DIUF water, 800 μL of 0.1 M CTAB, and 100 uL of 0.01 M $HAuCl_4$. A 600 μL portion of 0.1 M ascorbic acid was then added to the growth solution and mixed thoroughly, turning the solution colorless. Next, 2.5 μL of the diluted seed solution was added to the reaction vessel, and the solution was allowed to sit overnight. Nanocube solutions were purified using two rounds of centrifugation at 10 000 rpm for 10 min each. The final product was characterized by transmission electron microscopy, dynamic light scattering, and zeta potential (effective surface charge) analysis. Average cube size was 47 ± 3 nm, and the positive zeta potential (23.17 ± 2.23 mV) was consistent with a bilayer of CTAB on the surface, as we have postulated before.[28−30]

Nanoparticle Immobilization on SAMs. Gold substrates were prepared by sputtering 10 nm of chromium, followed by 100 nm of gold, on piranha-cleaned glass microscope slides cut to 1 cm^2. These slides were immersed in a 1 mM ethanolic solution of 4-MBA for 24 h to form the SAM on the gold surface.[17] After 24 h, the slides were rinsed thoroughly with ethanol and dried under nitrogen. A 20 mL solution of gold nanocubes was purified and resuspended in 4 mL of DIUF water. The gold-coated glass slides containing the SAMs of 4-MBA were immersed in 1 mL of the purified cube solution for 30 min, 1 h, 2 h, and 3 h to electrostaticaly bind the cubes to the SAM. The prepared slides were then rinsed with DIUF water and dried under nitrogen. Under these conditions, the 4-MBA SAM should be deprotonated to allow for electrostatic binding of the CTAB-capped gold nanocubes to the SAM surface.[17] Longer incubation times lead to higher surface coverages.

Surface Coverage and Aggregation Measurements. Nanocube surface coverage was calculated by dividing the total number of nanocubes counted in any given SEM field by the area of that field. Surface coverage values are reported as cubes/μm^2 and are averaged over three SEM micrographs for each incubation time. Estimates of percent aggregation were made using ImageJ analysis software, because counting the number of particles per aggregate was difficult by eye from the SEM micrographs. The known average area of a particle was compared to the size of SEM-observed aggregates to determine the number of particles present in each aggregate. Aggregates were defined as 2 or more particles separated by less than 10 nm. The percent aggregation for each sample was defined as the ratio of the number of nanocubes in aggregates to the total number of nanocubes per slide.

Calculation of Enhancement Factor. Surface enhancement factors (EF) were calculated for each of the different nanoparticle shapes using the following expression

$$\mathrm{EF} = (I_{\mathrm{SERS}})/(I_{\mathrm{Raman}}) \times (M_{\mathrm{bulk}})/(M_{\mathrm{ads}})$$

where M_{bulk} is the number of molecules sampled in the bulk, M_{ads} is the number of molecules adsorbed and sampled on the SERS-active substrate, I_{SERS} is the intensity of a vibrational mode in the surface-enhanced spectrum, and I_{Raman} is the intensity of the same mode in the Raman spectrum. For all spectra, the intensity of the CC ring-breathing mode (~1075 cm^{-1}) was used to calculate EF values. No Raman spectrum of the 4-MBA SAM without nanocubes was observed; therefore, the spectrum of aqueous 0.1 M 4-MBA was used to normalize the SERS data in the EF calculation. All spectra were normalized for acquisition time. The number of molecules sampled in the SERS experiments was determined by calculating the total two-dimensional area or "SERS footprint" occupied by the nanoparticles in the illuminated laser spot on the surface. This was approximated by multiplying the number density of nanoparticles (obtained using SEM images like those seen in Figure 3), the illuminated spot size, and the nanoparticle footprint area (from TEM images such as the one in Figure 1A) to give the total SERS surface area sampled. This number was multiplied by the bonding density of 4-MBA molecules in a SAM, ~0.5 nmol/cm^2, to give the total number of molecules sampled in the SERS experiments.

Results and Discussion

Nanocube Characterization and Immobilization. Figure 1A shows a typical transmission electron micrograph of the gold nanocubes used in this study; average particle size is 47 ± 3 nm. Figure 1B shows a high-resolution TEM image of a single gold nanocube, and its corresponding selected-area electron diffraction pattern is shown in Figure 1C. The electron diffrac-

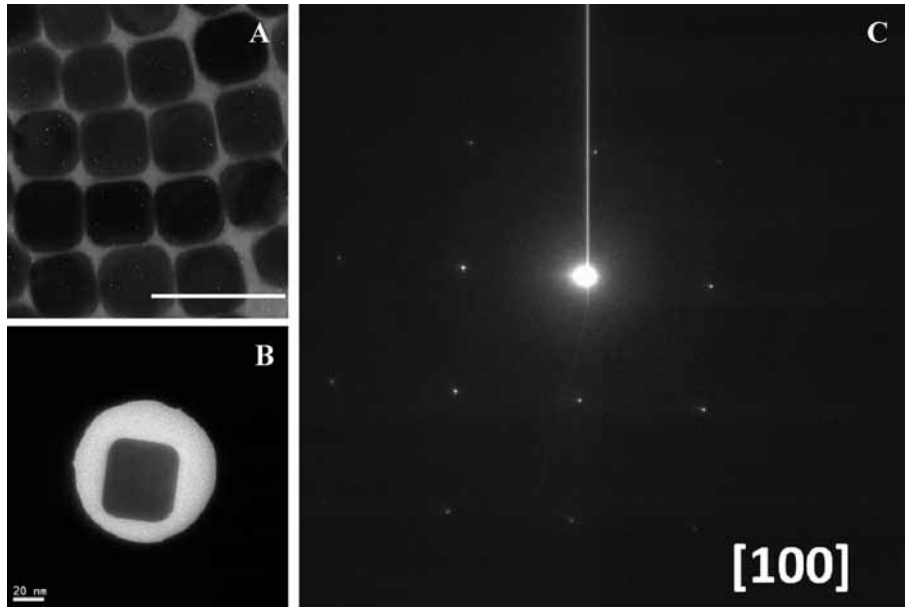

Figure 1. (A) Transmission electron micrograph of gold nanocubes. Scale bar = 100 nm. (B) High-resolution transmission electron micrograph of one of the gold nanocubes used for single-area electron diffration. Scale bar = 20 nm. (C) Representative diffraction pattern showing the {100} crystallographic facets of the nanocubes.

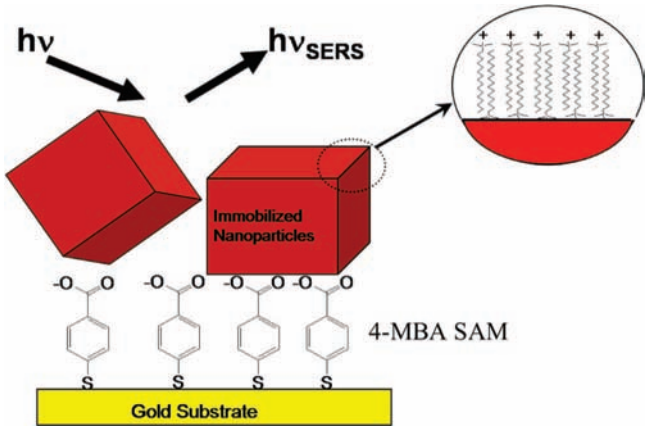

Figure 2. Scheme of the SAM-nanocube sandwich geometry used for obtaining SERS spectra of 4-MBA on smooth gold substrates. The circle zoom-in shows a schematic of the CTAB bilayer on the nanocube surface. Laser irradiation at either 633 or 785 nm results in SERS from the 4-MBA immobilized below the particles.

tion data suggest that the cubes are bounded by the {100} facets of gold, as others have observed before.[31] Gold cubes of edge lengths 47 ± 3 nm have only one plasmon band at ~545 nm, which does not have significant overlap with either of the laser lines used in the subsequent SERS experiments.

The gold nanocubes as made bear a bilayer of the structure-directing surfactant CTAB, which in turn imparts a high positive effective charge to the particles and leads to the trimethylammonium headgroup of CTAB facing the solvent.[30,32,33] The 4-MBA SAM displays the carboxylic acid group to the solvent, which is deprotonated under our conditions to allow for electrostatic immobilization of the nanocubes on the surface (Figure 2), as demonstrated previously.[28] Increasing incubation times of nanocube solutions with the SAMs led to increased surface coverage of the cubes on the SAMs. Figure 3 shows representative SEM images of gold nanocubes for the lowest (30-min incubation time; Figure 2A) and highest (3-h incubation time; Figure 2B) surface coverage and degree of aggregation. In Figure 2A, the gold nanocubes are distributed on the surface with a density of 5.5 cubes/μm^2, and we estimate ~14% of the cubes are aggregated, as we defined in the Experimental Section. In Figure 2B, the gold nanocubes are distributed on the surface with a density of 22 cubes/μm^2, and we estimate ~51% of the cubes are aggregated. The average number of nanocubes sampled within the spot sizes of the lasers for the 785 and 632.8 nm Raman systems range from 4.4 to 17 cubes for the 785 nm system and from 17 to 69 cubes for the 632.8 nm system, depending on surface coverage. It is not possible in the deposition process to separately control surface coverage and degree of aggregation; however, we can crudely separate out surface coverage from aggregation state using image analysis of the SEM images, as per the Experimental Section.

SERS of 4-MBA SAMs Using Gold Nanocubes at Varying Surface Coverages and Aggregation States. For these experiments, two different Raman microscopes were used, with laser lines at 632.8 or 785 nm. A set of five sample slides were made, ranging from a surface coverage of 0 to 22 cubes/μm^2, and analyzed using a 3 s acquisition time for the 632.8 nm Raman system and 120 s for the 785 nm Raman system. Raman spectra were recorded in triplicate from 100 areas of each slide and averaged to determine the representative Raman intensity from each slide. The results for each time point are highly reproducible over all areas of each chip for both laser lines. There are no characteristic 4-MBA vibrational signals for the SAM of 4-MBA for either laser line without immobilized gold nanoparticles, as we have observed before.[17] No CTAB Raman lines interfere with the 4-MBA signal, as we have observed before.[17] However, as the coverage of nanocubes on the surface of the chip is increased, the characteristic vibrational modes of 4-MBA begin to appear and increase in intensity (Figures 4 and 5). These modes include the stretching associated with the ring breathing modes at 1075 and 1581 cm^{-1}, the bending of the CH groups on the ring at 1152 and 1177 cm^{-1}, and the stretching associated with the carboxylate group at 1268 cm^{-1}. At sufficiently high nanocube coverages, the CH bending modes and carboxylate stretching modes are evident (Figures 4 and 5). Minor differences in the relative peak intensities at the two excitation wavelengths are observed, consistent with theoretical calculations of SERS spectra at two different excitation wavelengths.[34]

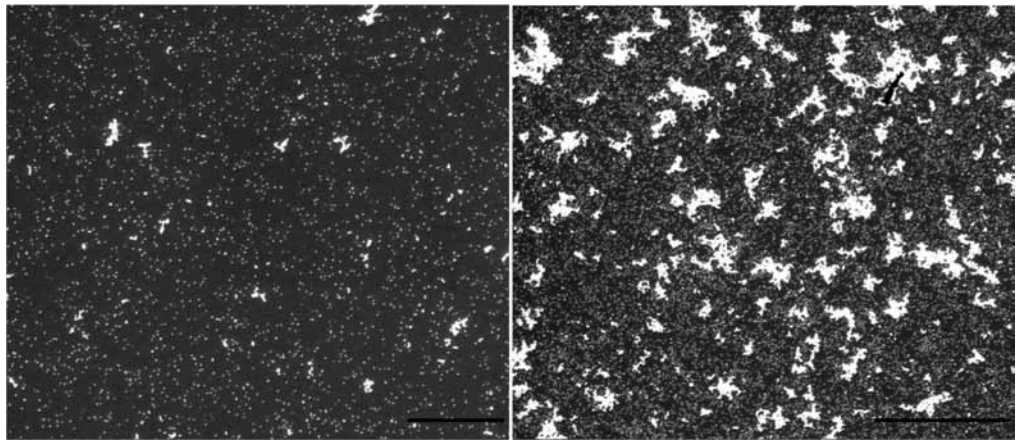

Figure 3. Scanning electron micrographs of (A) gold nanocubes electrostaticaly immobilized on 4-MBA SAM at 5.5 cubes/μm^2 with ~14% aggregation (scale bar = 5 μm); (B) gold nanocubes electrostaticaly immobilized on 4-MBA SAM at 22 cubes/μm^2 with ~51% aggregation (scale bar = 10 μm). The background is dark gray, and the nanocubes are white in this image mode.

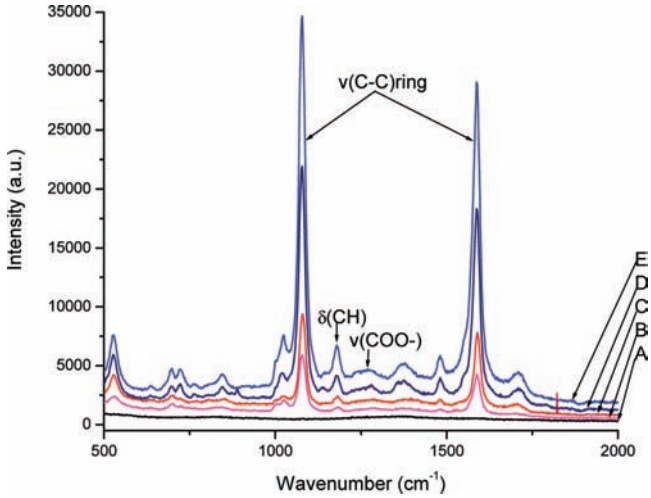

Figure 4. Raman spectra taken at 785 nm of the 4-MBA SAM: (A) alone (black line), (B) with 5.5 cubes/μm^2 at ~14% aggregation of cubes, (C) 8.6 cubes/μm^2 at ~42% aggregation of cubes, (D) 15 cubes/μm^2 at ~43% aggregation of cubes, and (E) 22 cubes/μm^2 at ~51% aggregation of cubes.

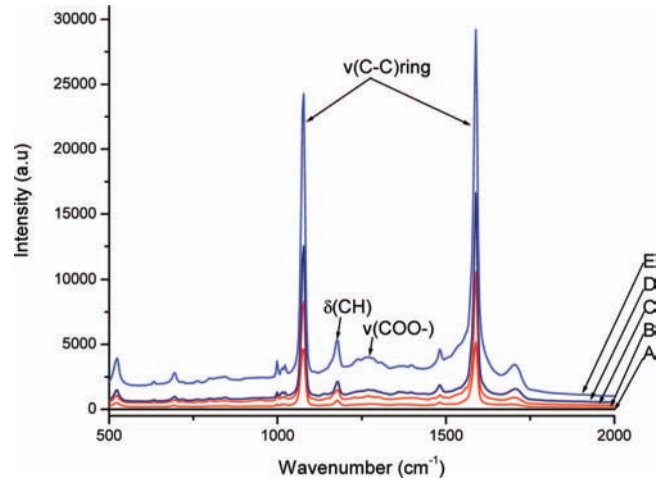

Figure 5. Raman spectra taken at 632.8 nm of of the 4-MBA SAM: (A) alone (black line), (B) with 5.5 cubes/μm^2 at ~14% aggregation of cubes, (C) 8.6 cubes/μm^2 at ~42% aggregation of cubes, (D) 15 cubes/μm^2 at ~43% aggregation of cubes, and (E) 22 cubes/μm^2 at ~51% aggregation of cubes.

Aggregation of noble metal nanoparticles in general is known to enhance SERS signals, although quantitation of this effect can be difficult to unravel. The Kneipp group has shown that aggregation of gold nanoparticles in solution can lead to enhancement of an analyte's SERS signal by 10 orders of magnitude over isolated gold particles.[16] Moskovits et al. estimate that junctions between supported silver spheres compared to small solution aggregates provide 100−1000× SERS signal intensities from molecules in the junction.[35] Previously, we have shown that SERS enhancement factors are 10^9 for gold nanocubes in the "0% aggregation state" on a flat gold surface, compared to the normal Raman spectrum of 4-MBA in aqueous basic solution (although those nanocubes were slightly larger than the ones made here).[17] Here, we increase the surface coverage of the nanocubes on the analyte SAM in order to start forming junctions between the nanocubes to increase SERS intensity and enhancement factor, assuming that the nanocube−nanocube junctions' increased electric field could be accessed by molecules underneath the nanocubes.

In solution, aggregation between gold nanocubes does lead to a decrease in the absorbance at ~545 nm and the growth of a broad peak centered at ~844 nm (Figure 6). Thus, increased nanocube absorbance on the SERS substrates due to aggregation is convoluted into the spectral response. We had expected that if we found that SERS signals increased in a simple linear manner with surface coverage, then the number of molecules sampled would be directly proportional to signal, and thus, the degree of surface-bound nanocube aggregation is likely irrelevant, perhaps because the increased local electric field is concentrated too far above the SAM. If the SERS signals increased exponentially (for example) as a function of surface coverage, then we would suspect that the increased nanocube aggregation that accompanies increased surface coverage would be responsible for these nonlinear effects.

Figure 7A and B shows SERS signal intensity vs surface coverage in cubes/μm^2 for the two laser lines used, and we indeed find that there is a linear relationship between SERS intensity and surface coverage for both 632.8 and 785 nm excitation. We note that in our system, not only is the analyte below the nanocubes, as can be seen schematically in Figure 2, but also the nanocubes contain a bilayer of CTAB on the surface which provides a ~2.4 nm spacer between the nanocubes and the analyte (although molecules may partition into this bilayer).[37] Our data support the work of Käll et al., who have calculated that the position of SERS hot spots between two particles (assuming no crevices) is concentrated in the middle of the nanoparticles and does not appreciably "leak" out to the particle

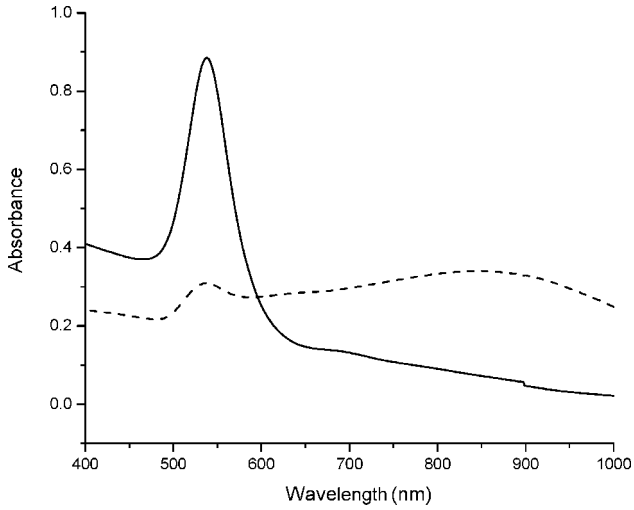

Figure 6. UV−vis−NIR absorption spectra of gold nanocubes: (—) before aggregation and (− −) after aggregation by increasing salt concentration.

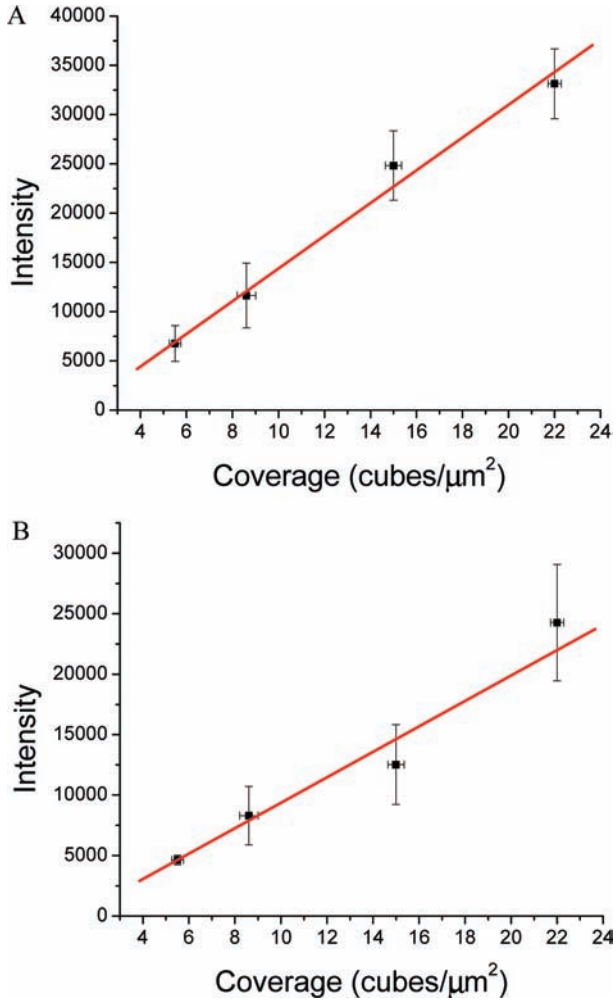

Figure 7. Dependence of Raman signal intensity on nanocube surface coverage: (A) nanocube coverage vs intensity for the 785 nm data (linear fit shown) and (B) nanocube coverage vs intensity for the 632.8 nm data (linear fit shown).

boundaries (although these effects probably depend on the absolute particle size, as well).[36] Excitation of identical samples at 785 nm does provide more of a signal boost than excitation at 632.8 nm, likely in part due to the increased absorbance of the sample at 785 nm compared to 632.8 nm (Figure 6). Enhancement factors also show this trend. The enhancement factors calculated from the data obtained at 785 nm range from $(3.1 \pm 0.3) \times 10^{12}$ to $(1.0 \pm 0.3) \times 10^{13}$, but those associated with the data obtained at 632.8 nm range from $(7.8 \pm 1.5) \times 10^{7}$ to $(4.1 \pm 0.4) \times 10^{8}$ (Table 1). The enhancement factors are also higher at 785 nm because free 4-MBA has weaker normal Raman signals at this excitation wavelength. The calculated enhancement factors apparently decrease slightly with increasing nanoparticle surface coverage, but these numbers are highly dependent on accurate estimations of molecules sampled. The far more significant parameter is choice of laser wavelength. In our previous work at 632.8 nm excitation, gold nanocubes of a slightly different size and lower surface coverages gave 10^{9}-fold enhancements, but here, 785 nm excitation adds orders of magnitude to the enhancement factors. Beyond this, mechanisms to improve SERS signals of molecules in our SAM geometry might include (i) using particles with sharper and perhaps more unusually shaped tips to funnel the local electric fields to the SAM and (ii) increasing the size of nanocubes so that they absorb more of the incident light.

TABLE 1: Calculated Surface Enhancement Factors (EF) for 4-MBA SAMs on Gold Substrates with Immobilized Gold Nanocubes

surface coverage (cubes/μm^2)	enhancement factor	
	785 nm excitation	633 nm excitation
14 ± 1	$1.0 \pm 0.3 \times 10^{13}$	$4.1 \pm 0.4 \times 10^{8}$
42 ± 1	$7.0 \pm 1.9 \times 10^{12}$	$2.2 \pm 0.7 \times 10^{8}$
43 ± 2	$5.5 \pm 0.8 \times 10^{12}$	$1.1 \pm 0.3 \times 10^{8}$
51 ± 3	$3.1 \pm 0.3 \times 10^{12}$	$7.8 \pm 1.5 \times 10^{7}$

Conclusion

This report offers a colloidal chemistry approach to maximize signal from SERS analytes adsorbed to planar substrates. Gold nanocubes were immobilized on SAMs of the Raman-active molecule 4-MBA on smooth gold substrates by electrostatic interactions. This creates a sandwich architecture in which the localized surface plasmon band of the gold nanocubes couples with the surface plasmon of the gold substrate, creating a large localized electromagnetic field enhancement. This electromagnetic field leads to an enhancement of the SERS signal from the 4-MBA SAM on the planar substrate. Without the nanocubes, the 4-MBS SAM has no detectable Raman signal, but upon addition of gold nanocubes, the bands associated with the ring breathing modes, the bending of the CH groups on the ring, and the stretching associated with the carboxylate groups all begin to appear. The data in this paper suggest that the intensity of these vibrational bands depends on the surface coverage of the nanoparticles, but not their aggregation state per se.

Acknowledgment. We thank Profs. M. Angel and C. Williams for use of their microRaman systems. We thank Dr. D. Blom for assistance with the HRTEM. This work was supported in part by the National Science Foundation, the U. S. Air Force, and the U. S. Department of Energy.

References and Notes

(1) Haynes, C. L.; Yonzon, C. R.; Zhang, X.; Van Duyne, R. P. *J. Raman Spectrosc.* **2005**, *36*, 471.
(2) Jeanmaire, D. L.; Van Duyne, R. P. *J. Electroanal. Chem.* **1977**, *84*, 1.
(3) Albrecht, M. G.; Creighton, J. A. *J. Am. Chem. Soc.* **1977**, *99*, 5215.
(4) Haynes, C. L.; McFarland, A. D.; Van Duyne, R. P. *Anal. Chem.* **2005**, 338A.
(5) Garrell, R. L. *Anal. Chem.* **1989**, *61*, 410A.

(6) Kneipp, K.; Kneipp, H.; Kneipp, J. *Acc. Chem. Res.* **2006**, *39*, 443.
(7) Campion, A.; Kambhampati, P. *Chem. Soc. Rev.* **1998**, *27*, 241.
(8) Lal, S.; Grady, N. K.; Kundu, J.; Levin, C. S.; Lassiter, J. B.; Halas, N. J. *Chem. Soc. Rev.* **2008**, *37*, 898.
(9) Lyon, l. A.; Keating, C. D.; Fox, A. P.; Baker, B. E.; He, L.; Nicewarner, S. R.; Mulvaney, S. P.; Natan, M. J. *Anal. Chem.* **1998**, *70*, 341R.
(10) Mulvaney, S. P.; Keating, C. D. *Anal. Chem.* **200**, *72*, 145R.
(11) Banholzer, M. J.; Millstone, J. E.; Qin, L.; Mirkin, C. A. *Chem. Soc. Rev.* **2008**, *37*, 885.
(12) El-Sayed, M. A. *Acc. Chem. Res.* **2001**, *34*, 257.
(13) Kelly, K. L.; Coronado, E.; Zhao, L. L.; Schatz, G. C. *J. Phys. Chem. B* **2003**, *107*, 668.
(14) Moskovits, M. *J. Raman Spectrosc.* **2005**, *36*, 485.
(15) Le Ru, E. C.; Grand, J.; Felidj, G. N.; Aubard, J.; Levi, G.; Hohenau, A.; Krenn, J. R.; Blackie, E.; Etchegoin, P. G. *J. Phys. Chem. C* **2008**, *112*, 8117.
(16) Kneipp, K.; Kneipp, H.; Manoharan, R.; Hanlon, E. B.; Itzkan, I.; Dasari, R. R.; Feld, M. S. *App. Spec.* **1998**, *52*, 1493.
(17) Orendorff, C. J.; Gole, A.; Sau, T.; Murphy, C. *J. Anal. Chem.* **2005**, *77*, 3261.
(18) Murphy, C. J.; Gole, A. M.; Hunyadi, S. E.; Stone, J. S.; Sisco, P. N.; Alkilany, A.; Kinard, B. E.; Hankins, P. *Chem. Commun.* **2008**, *5*, 544.
(19) Murphy, C. J.; Sau, T. K.; Gole, A. M.; Orendorff, C. J. *MRS Bulletin* **2005**, *30*, 349.
(20) Gersten, J. I. *J. Chem. Phys.* **1980**, *72*, 5779.
(21) Schatz, G. *Acc. Chem. Res.* **1984**, *17*, 370.
(22) Jeong, D. H.; Zhang, Y. X.; Moskovits, M. *J. Phys. Chem.* **2004**, *108*, 12724.
(23) Schierhorn, M.; Lee, S. J.; Boettcher, S. W.; Stucky, G. D.; Moskovits, M. *Adv. Mater.* **2006**, *18*, 2829.
(24) Nikoobakht, B.; Wang, J.; El-Sayed, M. A. *Chem. Phys. Lett.* **2002**, *366*, 17.
(25) Nikoobakht, B.; El-Sayed, M. A. *J. Phys. Chem. A* **2003**, *107*, 3372.
(26) Huang, X.; El-Sayed, I.; Qian, W.; El-Sayed, M. A. *Nano Lett.* **2007**, *7*, 1591.
(27) Jackson, J. B.; Halas, N. J. *Proc. Nat. Acad. Sci. U.S.A.* **2004**, *52*, 17930.
(28) Gole, A.; Orendorff, C. J.; Murphy, C. J. *Langmuir* **2004**, *20*, 7117.
(29) Sau, T. K.; Murphy, C. J. *J. Am. Chem. Soc.* **2004**, *126*, 8648.
(30) Murphy, C. J.; Sau, T. K.; Gole, A. M.; Orendorff, C. J.; Gao, J.; Gou, L.; Hunyadi, S. E.; Li, T. *J. Phys. Chem. B* **2005**, *109*, 13857.
(31) Elechiguerra, J. L.; Reyes-Gasga, J.; Yacaman, M. J. *J. Mater. Chem.* **2006**, *16*, 3906.
(32) Nikoobakht, B.; El-Sayed, M. A. *Langmuir* **2001**, *17*, 6368.
(33) Sau, T. K.; Murphy, C. J. *Langmuir* **2005**, *21*, 2923.
(34) Zhao, L. L.; Jensen, L.; Schatz, G. C. *Nano Lett.* **2006**, *6*, 1229.
(35) Braun, G.; Pavel, I.; Morrill, A. R.; Seferos, D. S.; Bazan, G. C.; Reich, N. O.; Moskovits, M. *J. Am. Chem. Soc.* **2007**, *129*, 7760.
(36) Xu, H.; Aizpurua, J.; Käll, M.; Apell, P. *Phys. Rev. E* **2000**, *62*, 4318.
(37) Alkilany, A. M.; Frey, R. L.; Ferry, J. L.; Murphy, C. J. *Langmuir* **2008**, *24*, 10235.

JP810329J